The Astrophysical Journal Letters, 841:L14 (5pp), 2017 May 20 https://doi.org/10.3847/2041-8213/aa71a6

Detection of HC_3N Maser Emission in NGC 253

Simon P. Ellingsen[1], Xi Chen[2,3], Shari L. Breen[4], and Hai-hua Qiao[2]
[1] School of Physical Sciences, University of Tasmania, Hobart, Tas 7001, Australia; Simon.Ellingsen@utas.edu.au
[2] Shanghai Astronomical Observatory, Chinese Academic of Sciences, Shanghai 200030, China
[3] Center for Astrophysics, GuangZhou University, Guangzhou 510006, China
[4] Sydney Institute for Astronomy (SIfA), School of Physics, University of Sydney, Sydney, NSW 2006, Australia
Received 2017 April 18; revised 2017 May 4; accepted 2017 May 6; published 2017 May 22

Abstract

We report the detection of maser emission from the $J = 4$–3 transition of HC_3N at 36.4 GHz toward the nearby starburst galaxy NGC 253. This is the first detection of maser emission from this transition in either a Galactic or extragalactic source. The HC_3N maser emission has a brightness temperature in excess of 2500 K and is offset from the center of the galaxy by approximately 18″ (300 pc), but close to a previously reported class I methanol maser. Both the HC_3N and methanol masers appear to arise near the interface between the galactic bar and the central molecular zone, where it is thought that molecular gas is being transported inwards, producing a region of extensive low-velocity shocks.

Key words: galaxies: individual (NGC 253) – galaxies: starburst – masers – radio lines: ISM

1. Introduction

NGC 253 is the largest galaxy in the Sculptor group and is one of the closest galaxies with a nuclear starburst, at a distance of 3.4 Mpc (Dalcanton et al. 2009). The disk of the galaxy has a relatively high inclination angle to our line of sight (72°–78°; Puche et al. 1991) and shows strong molecular emission from a wide range of species (e.g., Martín et al. 2006). It has been the object of detailed studies across the electromagnetic spectrum from radio through to γ-ray (e.g., Ulvestad & Antonucci 1997; Weiß et al. 2008; Dale et al. 2009; Sakamoto et al. 2011; Lehmer et al. 2013; Iodice et al. 2014).

NGC 253 hosts both water masers associated with star formation within the nuclear ring (Henkel et al. 2004; Hofner et al. 2006) and OH maser emission associated with the nuclear outflow (Turner 1985). There is also evidence for the presence of an $NH_3(3,3)$ maser toward the center (Ott et al. 2005). Phillips et al. (1998) searched for class II 6.7 GHz methanol masers toward NGC 253, but did not detect any emission (5-σ sensitivity limit of ∼110 mJy). Most recently, the first detection of extragalactic class I methanol maser emission from the 36.2 GHz $4_{-1} \rightarrow 3_0 E$ transition was reported toward NGC 253 (Ellingsen et al. 2014).

HC_3N is a linear molecule first detected in interstellar space by Turner (1971) toward the Sgr B2 molecular cloud. Although it has a wide range of observable transitions at centimeter and millimeter wavelengths and its astrophysical importance has long been recognized (Morris et al. 1976), it has been relatively poorly studied. The first interstellar detection of the $J = 4$–3 transition at 36.4 GHz was toward Sgr B2 (McGee et al. 1977). Modeling of multi-transitional HC_3N data toward Sgr B2 suggests that it arises from gas with a kinetic temperature of around 20 K and number density $>10^5$ cm^{-3} (Brown & Cragg 1985). More recently, observations of vibrationally excited states of HC_3N have been used to investigate hot molecular cores (HMC). Wyrowski et al. (1999) find the population distribution of the HC_3N to be consistent with gas kinetic temperatures around 270 K and that it is located close to classical HMC molecular tracers such as CH_3CN. Early observations of HC_3N in Sgr B2 noted the $J = 1$–0 transition showed anomalously strong emission (Morris et al. 1976) and it was subsequently confirmed to be a weak maser from higher angular resolution observations (Hunt et al. 1999). However, the 9.1 GHz $J = 1$–0 HC_3N emission in Sgr B2 is to date the only reported interstellar maser in this molecule. Here, we report the first high-resolution images of HC_3N toward the central region of NGC 253.

2. Observations

The Australia Telescope Compact Array (ATCA) was used to observe NGC 253 on 2014 October 10 and November 27 (project code C2879). The array was in the 1.5A configuration (baseline lengths between 153 and 1469 m) for the October session and in the EW367 (baseline lengths between 46 and 367 m) for the November session. The Compact Array Broadband Backend (Wilson et al. 2011) was configured with 2×2048 MHz bands, both centered at a frequency of 36.9 GHz. One of the 2048 MHz bands had 2048×1 MHz spectral channels, while the other had two "zoom-bands" with spectral channels of width 31.25 kHz and a bandwidths of 128 MHz (corresponding to 4096 channels per zoom-band). The primary purpose of these observations was to investigate the class I methanol maser emission previously observed in NGC 253 (Ellingsen et al. 2014) and a detailed investigation of those data will be presented in a forthcoming paper. The 2048×1 MHz band includes the rest frequency of the $J = 4$–3 transition of HC_3N (36.392332 GHz), which has six hyperfine components that are spread over a frequency range of 3.3 MHz. Of the six hyperfine components only the $F = 3$–2, $F = 4$–3 and $F = 5$–4 are expected to be significant in interstellar observations (McGee et al. 1977), and these span a frequency range of 0.13 MHz, significantly less than the 1 MHz spectral resolution of the current observations.

The data were reduced with MIRIAD following the standard data reduction techniques for ATCA observations. Amplitude calibration was with respect to Uranus and PKS B1921−293 was observed as the bandpass calibrator. The data were corrected for atmospheric opacity and the absolute flux density calibration is estimated to be accurate to 30%. The observing strategy interleaved 10 minutes on NGC 253 (pointing center $\alpha = 00^h47^m33^s.10$; $\delta = -25°17'18''.0$ (J2000)) with 2-minute

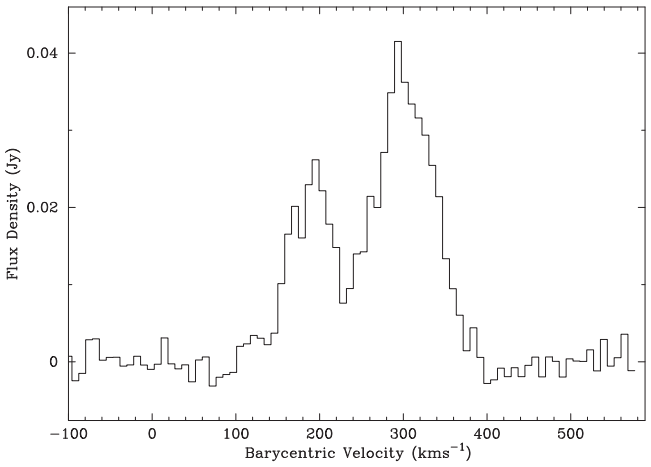

Figure 1. ATCA spectrum of the integrated 36.4 GHz HC_3N emission from NGC 253, extracted from the combined array image cube.

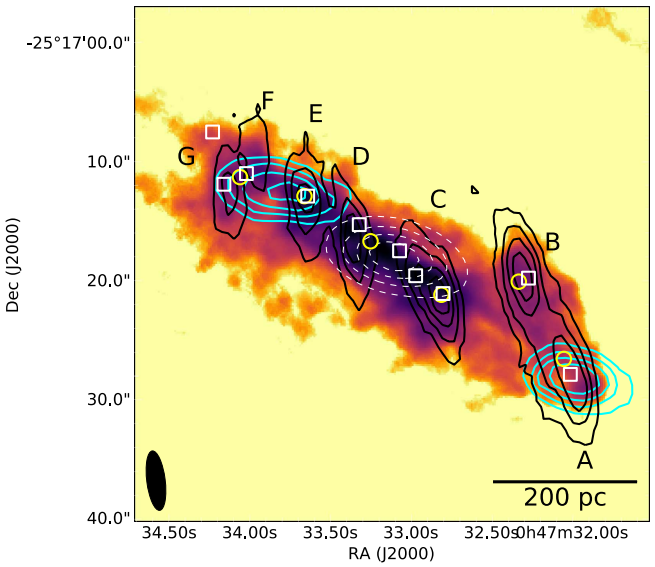

Figure 2. ATCA combined EW367 and 1.5A array observations of the HC_3N emission toward NGC 253 (black contours at 20%, 40%, 60%, and 80% of 497 mJy km s^{-1} beam^{-1}, synthesized beam 5.″0 × 1.″5, image rms 15 mJy km s^{-1} beam^{-1}). 36 GHz continuum emission (dashed white contours at 20%, 40%, 60%, and 80% of 95 mJy beam^{-1}) and 36.2 GHz methanol emission (cyan contours at 20, 40, 60 and 80% of 310 mJy km s^{-1} beam^{-1}) toward the central molecular zone in NGC 253 (Ellingsen et al. 2014). The background image is the integrated CO ($J = 2 - 1$) emission from Sakamoto et al. (2011) shown on a logarithmic scale. The white squares mark the location of molecular clouds identified by Leroy et al. (2015) and the yellow circles the location of NH_3 sources (Lebrón et al. 2011).

observations of a nearby phase calibrator (0116-219) before and after the target source. The total duration onsource for NGC 253 was around 4–5 hr for each array configuration. The data from each ATCA array configuration were calibrated and reduced independently. The strong continuum emission from the central region of NGC 253 was then used to self-calibrate the data from each session, prior to continuum subtraction. This significantly improves the signal to noise for both the continuum and line data sets. The rms noise levels in the HC_3N cubes (1 MHz, or 8.2 km s^{-1} channel width) was 0.4 mJy beam^{-1}, 0.3 mJy beam^{-1} and 0.3 mJy beam^{-1} for the EW367, 1.5A and combined array data, respectively.

To investigate the compact emission from the HC_3N $J = 4$–3 transition, we used the Jansky Very Large Array (JVLA) in A-array configuration to make observations of this line toward NGC 253 on 2015 August 13. Two 1 GHz bands (8-bit samplers) with frequencies centered at around 36.1 GHz and 37.1 GHz were used for these observations. Each band included 8 × 128 MHz dual polarization sub-bands, with 128 spectral channels each of 1 MHz. The HC_3N transition was located in a sub-band centered at 36.396 GHz. The calibration of the time-dependent antenna gains was performed by frequent observations of the quasar J0025-2602. J2253+1608 (3C454.3) was used to calibrate the bandpass response and the absolute flux density scale was determined through observations of 3C48. The pointing center for the JVLA observations of NGC 253 was the same as for the ATCA observations and the onsource integration time was about 1 hour. The visibility data were calibrated using the standard JVLA Calibration Pipeline[5] with the Common Astronomy Software Applications (CASA) package. The imaging and analysis were carried out in MIRIAD. The synthesized beam size for the image is 0.″16 × 0.″07 with a position angle of −28° northwest. Similar to the ATCA data reduction, self-calibration using the continuum emission from NGC 253 was performed prior to continuum subtraction.

3. Results

The continuum subtracted data from the two ATCA array configurations were combined during imaging, to improve both the overall sensitivity and the range of angular scales for which information is available. Figure 1 shows the spectrum of the integrated 36.4 GHz HC_3N emission, extracted from the combined array ATCA image cube. The integrated emission is 4.6 Jy km s^{-1} and covers a Barycentric velocity range from approximately 150–380 km s^{-1}. Figure 2 shows the spatial distribution of the 36.4 GHz HC_3N emission from the ATCA observations, along with a range of other molecular tracers. Recent ALMA observations of NGC 253 have given us high-resolution (2.″0 × 1.″5) information on the molecular gas content in the central regions of NGC 253 in a wide range of different molecules and transitions (Leroy et al. 2015; Meier et al. 2015). Leroy et al. identified 10 regions with significant volumes of dense gas, and these are marked with white squares in Figure 2. The highest angular resolution ATCA HC_3N observations have an angular resolution of around 2″, which corresponds to a linear scale of approximately 30 pc (assuming a distance of 3.4 Mpc to NGC 253) and the combined array ATCA observations show 7 distinct regions of emission. We have labeled these regions A through G in order of increasing right ascension (Figure 2). Table 1 summarizes the properties of the 7 HC_3N emission regions and their relationship to recent ALMA molecular line observations (Leroy et al. 2015; Meier et al. 2015). The HC_3N emission regions are generally offset by 0.″5–1″ from the ALMA-identified molecular cloud complexes, this is comparable to the relative astrometric uncertainty between the two data sets and so they are either associated, or in close proximity. The 7 HC_3N regions encompass nine of the 10 molecular complexes identified in the ALMA observations of (Leroy et al. 2015). Figure 2 shows that HC_3N region A is is close to the location of the strongest 36.2 GHz class I

[5] See https://science.nrao.edu/facilities/vla/data-processing/pipeline.

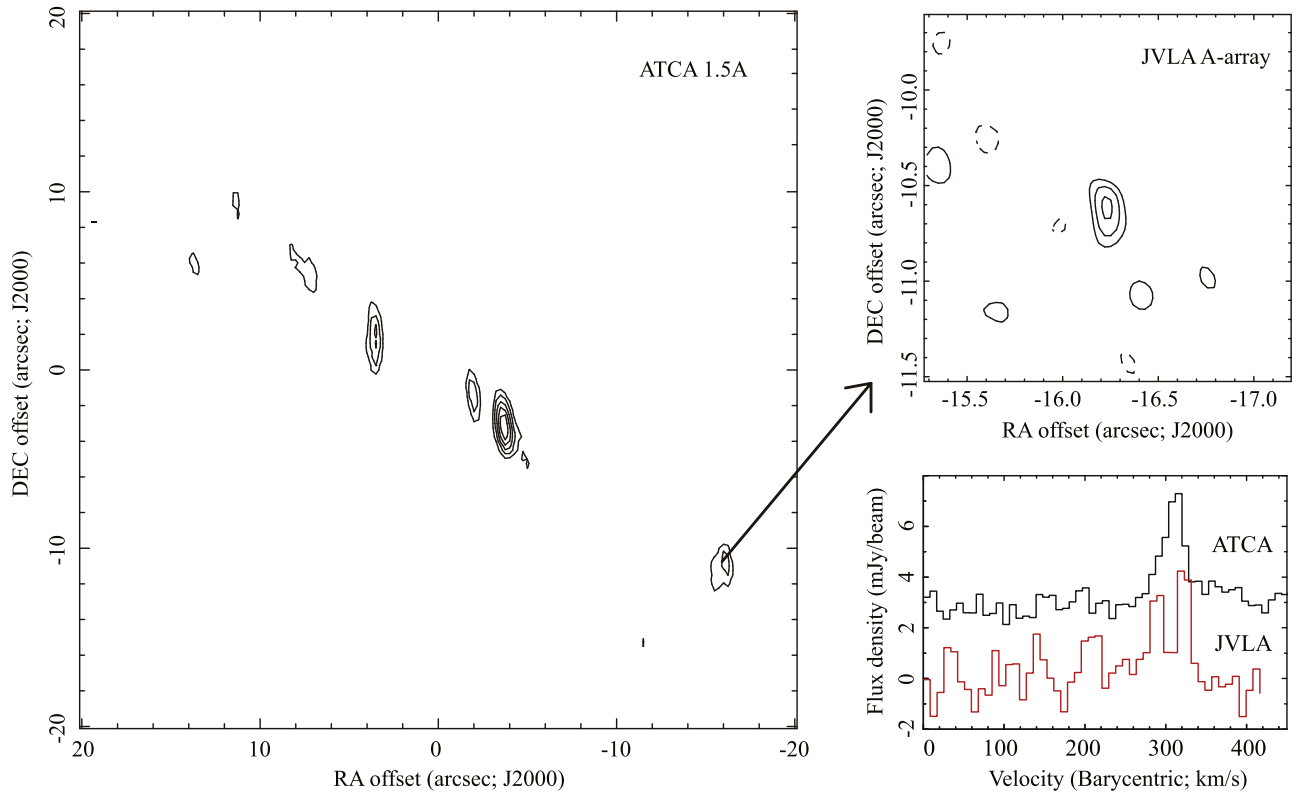

Figure 3. ATCA 1.5A array and JVLA A-array observations of the integrated $J = 4$–3 HC_3N emission. The contour levels in the ATCA image are at −3, 3, 5, 7, 9, and 11 times the rms in the image (15 mJy beam^{-1} km s^{-1}) The contour levels in the JVLA image are at −3, 3, 4, and 5 times the rms in the image (25 mJy beam^{-1} km s^{-1}). The JVLA observations covered the same field of field of view as the ATCA, but emission was only detected toward one of the emission sites observed at lower angular resolution.

Table 1
Summary of HC_3N Emission Regions in NGC 253

HC_3N source	R.A. (J2000)	Decl. (J2000)	Peak Velocity (km s^{-1})[a]	Velocity Range (km s^{-1})[a]	Integrated Flux (mJy km s^{-1})[b]	Leroy et al. cloud[c]	Meier et al. region[c]
A	00:47:31.98	−25:17:28.7	310	277–343	294	1 (1.″0)	3 (0.″7)
B	00:47:32.30	−25:17:20.4	335	253–360	439	2 (0.″8)	2 (1.″3)
C	00:47:32.82	−25:17:21.4	294	261–318	443	3 (0.″5)	4 (0.″5)
D	00:47:33.37	−25:17:16.1	179	154–203	275	6 (1.″1)	7 (0.″9)
E	00:47:33.62	−25:17:12.4	187	146–220	257	7 (0.″5)	8 (0.″8)
F	00:47:33.94	−25:17:09.6	212	187–220	101	8 (1.″7)	9 (1.″5)
G	00:47:34.13	−25:17:12.7	212	187–261	166	9 (1.″0)	10 (0.″5)

Notes.
[a] Note that all the velocities in this paper are given in the Barycentric reference frame, which for NGC 253 are 7.24 km s^{-1} lower than the equivalent velocity in the local-standard of rest (LSR) frame.
[b] The integrated flux density and velocity range reported are measured over the synthesized beam of the ATCA combined array data at the location given (Figure 2).
[c] The value in brackets gives the offset from the measured HC_3N position.

methanol maser in NGC 253 (Ellingsen et al. 2014), with an offset between the two of 0.″75, corresponding to a linear separation of approximately 12 pc.

In addition to the images formed using the combined data from the two ATCA configurations, we also examined the images of the HC_3N emission from each configuration separately. The 1.5A array observations have a synthesized beam size of 2.″6 × 0.″6 and at this resolution much of the HC_3N emission is resolved (Figure 3). The two innermost HC_3N regions that are strongest in the combined image remain the strongest in the higher-resolution image; however, what is more striking is that some emission from the weaker, outer sites remains and this emission correlates closely with the 36.2 GHz class I methanol maser emission. The JVLA A-array observations have an order of magnitude higher angular resolution (0.″1) and in this data the HC_3N detection is detected from only one location. The detection is statistically marginal, at 5σ in the integrate intensity (moment 0) image and 4σ in the strongest spectral channel. However, we are confident that the detection is robust, as it matches both the position and velocity of the

peak observed in the ATCA observations (Figure 3). For the assumed distance to NGC 253 an angular resolution of 0.″1 corresponds to a linear scale of 1.6 pc.

4. Discussion

A useful place to commence our investigation of the detected HC_3N emission in NGC 253 is to compare our results with those from Galactic sources. However, there are relatively few published observations of HC_3N in Galactic sources and even fewer that report data on the $J = 4$–3 transition. One of the best-studied sources is the star-forming complex Sgr B2, which has been observed in a wide range of HC_3N transitions (e.g., McGee et al. 1977; Hunt et al. 1999). Early observations of this source noted that the $J = 1$–0 transition showed an anomalously high intensity compared to the higher J lines and weak maser emission in this line was subsequently confirmed by high-resolution observations (Hunt et al. 1999). However, to our knowledge, the $J = 1$–0 emission in Sgr B2 is to date the only HC_3N maser emission reported in the published literature.

The $J = 4$–3 emission in Sgr B2 has a peak intensity of 1.25 K and a full-width at half maximum of 25 km s^{-1} (McGee et al. 1977), which corresponds to an integrated flux density of approximately 660 Jy km s^{-1} (assuming 20 Jy/K for the Parkes 36 GHz observations). Assuming a distance of 7.9 kpc for Sgr B2 (Reid et al. 2009) and 3.4 Mpc for NGC 253 (Dalcanton et al. 2009), we find that the total HC_3N $J = 4$–3 emission in NGC 253 (integrated flux density 4.6 Jy km s^{-1}) is approximately 1300 times more luminous than that observed from the Sgr B2 complex. Wyrowski et al. (1999) present data from the vibrational ground state of the $J = 4$–3 HC_3N transition toward the HMC source G 10.47+0.03, but the focus of their paper is the vibrationally excited states, so few details are given of this transition. However, it appears that the emission is more than an order of magnitude weaker than that observed toward Sgr B2 in the same transition. The star formation rate in NGC 253 (4.2 $M_\odot$ yr^{-1}; Sanders et al. 2003), is significantly higher than in the Milky Way (0.7–1.5 $M_\odot$ yr^{-1}; Robitaille & Whitney 2010), and approximately 50% of this is concentrated in the central region of NGC 253. However, even though Sgr B2 is sometimes described as a mini-starburst, it is clear that the luminosity of the HC_3N in NGC 253 is much larger than can be explained through linear scaling with the star formation rate.

The ALMA observations of Meier et al. (2015) included the $J = 11$–10 HC_3N transition at 100.1 GHz and it shows a similar distribution to that seen in the ATCA combined array image (Figure 2). The spatial distribution of the HC_3N is also similar to that observed in HCN and some other thermal molecular lines. Comparing the HC_3N emission in Figures 2 and 3, it is clear that the much of the emission is resolved in the higher angular resolution observations, suggesting it is thermal. However, some of the HC_3N emission associated with region A is much more compact. Considering just the HC_3N $J = 4$–3 emission detected in the ATCA observations of region A, at an angular resolution of 1.″2 (1.5A array observations) it has an integrated flux density of 285 mJy km s^{-1}, corresponding to a luminosity a factor of 80 greater than Sgr B2. At the angular resolution of the JVLA A-array observations, we have integrated emission of approximately 200 mJy km s^{-1} from a region of 0.″1, corresponding to a luminosity more than 55 times that of Sgr B2, but arising from a smaller region (0.″1 corresponds to a linear scale of 1.6 pc for a distance of 3.4 Mpc). From the JVLA A-array observations we can put a lower limit on the brightness temperature of the HC_3N emission of >2500 K integrated over a 50 km s^{-1} velocity range (>560 K in the peak spectral channel). Ott et al. (2005) found kinetic temperatures in the range 150–200 K for the molecular clouds in the central region of NGC 253 from ATCA NH_3 observations (angular resolution 19″ × 5″), consistent with H_2 excitation temperatures of ∼200 K for the NGC 253 molecular gas determined from infrared observations (Rigopoulou et al. 2002). In contrast, based on data from a large number of thermal molecular transitions Meier et al. (2015) estimate kinetic temperatures around 80 K in the inner molecular clouds in NGC 253 (those associated with HC_3N regions C and D). They also measured excitation temperatures in the range 10–75 K for the NGC 253 central molecular clouds from two SO transitions in their ALMA data, and radiative transfer modeling inferred similar results. For HC_3N the critical density is 5 × 10^5 cm^{-3} (Green & Chapman 1978), approximately an order of magnitude higher than the density inferred through modeling of line intensity ratios in NGC 253 by Meier et al. (2015). Transitions with critical densities higher than the gas density will have excitation temperatures lower than the kinetic temperature, so we expect the excitation temperatures for HC_3N in NGC 253 to be <200 K. Meier et al. (2015) also found that the excitation temperatures in molecular gas at larger galactocentric radii were lower than for those closer to the nucleus. Hence, the brightness temperatures we measured for the compact HC_3N $J = 4$–3 emission in region A are significantly in excess of the thermal or excitation temperatures expected in NGC 253. This is strong evidence that some of the $J = 4$–3 emission from HC_3N region A in NGC 253 is being produced by a non-thermal process (i.e., it is a maser).

The most widely studied extragalactic masers are the 22 GHz water megamasers and the 1.6 GHz OH megamasers. The water megamasers are very compact and have been used to investigate kinematics and dynamics of the circumnuclear region of active galaxies at very high angular resolution (e.g., Argon et al. 2007). The OH megamasers are less well studied at high angular resolution, but it is clear that some of the maser emission arises in larger-scale (10–100 pc) diffuse regions (e.g., Rovilos et al. 2003). This also appears to be the case for extragalactic H_2CO masers (Baan et al. 2017) and class I methanol (Chen et al. 2015). The majority of the $J = 4$–3 HC_3N emission in NGC 253 is likely thermal, but it may be that some of the emission which is resolved in the higher angular data presented here is from larger-scale, diffuse maser regions, with the emission detected in the JVLA A-array observations representing just the most compact components of a larger maser emission region.

Brown & Cragg (1985) modeled the HC_3N emission in Sgr B2 based on multi-transition single dish data. They found that at modest densities ($n_{H_2} \sim 10^{2.5}$–10^5 cm^{-3}), the $J = 1$–0 transition can exhibit maser emission for a wide range of temperatures. Inversion in higher J transitions was shown to occur for a more restricted range of temperatures and densities, shifting to higher values of each as J increased. This is because HC_3N is inverted under conditions where neither collisional nor radiative processes dominate and more transitions invert as the temperature increases (radiative input) and the density increases (collisional input). The highest energy transition for which they found inversion in their model was the $J = 4$–3 for which they predict maser emission only for kinetic

temperatures >50 K and densities in a narrow range around $n_{H_2} \sim 10^{4.2}$ cm^{-3}. These temperatures and densities are broadly consistent with the values measured in the molecular clouds in NGC 253 by Meier et al. (2015; 80 K, $10^{4.75}$ cm^{-3}) and others.

The HC_3N maser emission in NGC 253 arises within molecular cloud complex 1 from the Leroy et al. (2015) study. This region covers a larger spatial scale and shows broader line profiles in both quiescent molecular gas and dense gas tracers than the other molecular cloud complexes they identify (see their Figure 10). The NGC 253 molecular clouds are highly supersonic and have surface densities that are comparable with those observed in the Milky Way Galactic center clouds, but are observed out to much larger galactocentric radii (Leroy et al. 2015), and it is speculated that these characteristics result in more efficient star formation. The Meier et al. (2015) study examined the ratio of HNCO to SiO toward a number of regions in NGC 253. SiO is thought to be produced from sputtering of grains in high velocity shocks, while HNCO is produced by dust ice mantle sublimation which requires weak shocks. Meier et al. (2015) found the HNCO:SiO ratio to be enhanced in the molecular clouds at higher galactocentric radii (their regions 2, 3, 9 and 10 which correspond to HC_3N regions B, A, F, and G respectively). They hypothesize that these are regions where weak shocks dominate and are similar to conditions observed in bar shock regions of other nearby spirals such as IC342 and Maffei 2, suggesting that they may be high-priority targets for future searches.

5. Conclusions

High-resolution observations of the 36.4 GHz $J = 4$–3 transitions of HC_3N in NGC 253 have detected weak maser emission offset from the nucleus of the galaxy. This emission appears to be associated with a region of the galaxy close to the inner edge of the bar, where there is a significant abundance of molecular gas and widespread low-velocity shocks. The present observations of $J = 4$–3 HC_3N maser emission are limited to a single source, so we are limited in our inferences. However, based on the information in the literature, it would appear that lower J transitions of HC_3N may show more widespread maser emission in NGC 253 and that sources where bar shocks are observed may be likely targets to find other HC_3N masers. Understanding the physical significance of HC_3N masers requires observations of additional sources and transitions to enable a better characterization of the emission properties and their relationship with the host galaxy and we encourage further studies to facilitate this.

The Australia Telescope Compact Array is part of the Australia Telescope National Facility which is funded by the Commonwealth of Australia for operation as a National Facility managed by CSIRO. X.C. acknowledges support from National Natural Science Foundation of China (NSFC) through grant NSFC 11590781. This research made use of NASA's Astrophysics Data System Abstract Service. This research has made use of the NASA/IPAC Extragalactic Database (NED) which is operated by the Jet Propulsion Laboratory, California Institute of Technology, under contract with the National Aeronautics and Space Administration.

References

Argon, A. L., Greenhill, L. J., Reid, M. J., Moran, J. M., & Humphreys, E. M. L. 2007, ApJ, 659, 1040
Baan, W. A., An, T., Klöckner, H.-R., & Thomasson, P. 2017, MNRAS, in press
Brown, R. D., & Cragg, D. M. 1985, MNRAS, 215, 395
Chen, X., Ellingsen, S. P., Baan, W. A., et al. 2015, ApJL, 800, L2
Dalcanton, J. J., Williams, B. F., Seth, A. C., et al. 2009, ApJS, 183, 67
Dale, D. A., Cohen, S. A., Johnson, L. C., et al. 2009, ApJ, 703, 517
Ellingsen, S. P., Chen, X., Qiao, H.-H., et al. 2014, ApJL, 790, L28
Green, S., & Chapman, S. 1978, ApJS, 37, 169
Henkel, C., Tarchi, A., Menten, K. M., & Peck, A. B. 2004, A&A, 414, 117
Hofner, P., Baan, W. A., & Takano, S. 2006, AJ, 131, 2074
Hunt, M. R., Whiteoak, J. B., Cragg, D. M., White, G. L., & Jones, P. A. 1999, MNRAS, 302, 1
Iodice, E., Arnaboldi, M., Rejkuba, M., et al. 2014, A&A, 567, A86
Lebrón, M., Mangum, J. G., Mauersberger, R., et al. 2011, A&A, 534, A56
Lehmer, B. D., Wik, D. R., Hornschemeier, A. E., et al. 2013, ApJ, 771, 134
Leroy, A. K., Bolatto, A. D., Ostriker, E. C., et al. 2015, ApJ, 801, 25
Martín, S., Mauersberger, R., Martín-Pintado, J., Henkel, C., & García-Burillo, S. 2006, ApJS, 164, 450
McGee, R. X., Newton, L. M., & Balister, M. 1977, MNRAS, 180, 585
Meier, D. S., Walter, F., Bolatto, A. D., et al. 2015, ApJ, 801, 63
Morris, M., Turner, B. E., Palmer, P., & Zuckerman, B. 1976, ApJ, 205, 82
Ott, J., Weiss, A., Henkel, C., & Walter, F. 2005, ApJ, 629, 767
Phillips, C. J., Norris, R. P., Ellingsen, S. P., & Rayner, D. P. 1998, MNRAS, 294, 265
Puche, D., Carignan, C., & van Gorkom, J. H. 1991, AJ, 101, 456
Reid, M. J., Menten, K. M., Zheng, X. W., Brunthaler, A., & Xu, Y. 2009, ApJ, 705, 1548
Rigopoulou, D., Kunze, D., Lutz, D., Genzel, R., & Moorwood, A. F. M. 2002, A&A, 389, 374
Robitaille, T. P., & Whitney, B. A. 2010, ApJL, 710, L11
Rovilos, E., Diamond, P. J., Lonsdale, C. J., Lonsdale, C. J., & Smith, H. E. 2003, MNRAS, 342, 373
Sakamoto, K., Mao, R.-Q., Matsushita, S., et al. 2011, ApJ, 735, 19
Sanders, D. B., Mazzarella, J. M., Kim, D.-C., Surace, J. A., & Soifer, B. T. 2003, AJ, 126, 1607
Turner, B. E. 1971, ApJL, 163, L35
Turner, B. E. 1985, ApJ, 299, 312
Ulvestad, J. S., & Antonucci, R. R. J. 1997, ApJ, 488, 621
Weiß, A., Kovács, A., Güsten, R., et al. 2008, A&A, 490, 77
Wilson, W. E., Ferris, R. H., Axtens, P., et al. 2011, MNRAS, 416, 832
Wyrowski, F., Schilke, P., & Walmsley, C. M. 1999, A&A, 341, 882